WATER-OIL RELATIVE PERMEABILITY IN VUGULAR POROUS MEDIA: EXPERIMENTS AND SIMULATIONS

A. Moctezuma-Berthier[1,2], O. Vizika[1], and P. Adler[3]
1. Institut Français du Pétrole, Rueil Malmaison, France, 2. Instituto Mexicano del Petróleo, México, D.F. México, 3. Institut de Physique du Globe, Paris, France.

ABSTRACT

In carbonated rocks, porosity is characterized by the superposition of several sizes of pores. Vug porosity influences the fluid flow characteristics of the rocks. This is because the vuggy system affects the way in which the main flowing pore system is connected. Within the vuggy rock two structures coexist: one corresponds to the macropores (or vugs), the other corresponds to the micropores. Permeability is controlled by the pore-size distribution but also by the interconnectivity between these two structures. Consequently, transport properties of multiphase flow in these porous media are expected to highly depend on the structure particularities.

The objective of this paper is to measure water-oil relative permeabilities in vugular porous media and to analyze them in terms of pore structure characteristics. To this end, water-oil injections (imbibition and secondary drainage conditions) in two different types of bimodal pore structure porous media were conducted, and single porosity 1D simulations were used to determine the relative permeability. The porous media used had comparable porosity and formation factor but very different structure. CT-scan local saturation measurements permitted to follow the water-oil front form and evolution for the different porous media.

The experimental results show very different imbibition patterns in terms of breakthrough time and recovery kinetics. CT-scan saturation profiles show the influence of double porosity system and its interconnectivity. 1D double porosity simulations demonstrated that production kinetics and saturation profiles can be successfully fitted with different and rather contrasted relative permeabilities for the macropore and micropore systems.

INTRODUCTION

The interpretation of multiphase flow experiments in reservoir rocks for the determination of transport properties and recovery factors has been the subject of a multitude of papers. The complex pore structure, the interfacial properties of the fluids and the interactions between fluids and solid surface have to be properly taken into account. Particularly in carbonates the porous structure is characterized by the presence of primary and secondary systems, resulting from diagenesis, and accurate estimation of the flow behavior in these type of media is not an easy task.

The definition of the large pores depends on the scale to which we are referring; usually at the core level, the pores of large size, i.e., of millimeter scale are called "vugs". On the well level, the large pores are called “vugs” if they are at the centimeter scale, or "cavern" if they are at the meter scale. Hence, for a given scale, two interconnected media may coexist, one corresponding to the macropores, the other corresponding to the micropores. Archie’s classification (1952) considered that pores could be divided into matrix porosity

and “visible” porosity (macropores). From Lucia’s classification (1999), vug porosity is defined as the “space” between grains and minerals that are normally considered as dissolved grains, fossil chambers, and fractures. Such systems are then connected in some way to a microporosity system.

The capacity of oil, water and gas to move in the reservoir is described using the relative permeabilities. Relative permeabilities play a key role in numerical simulation, and it is very important to understand the factors that influence their forms. Their determination is usually performed considering that core samples are “homogeneous”. Homogenous means that the length scale of heterogeneities of pore morphology is much smaller than the scale of observation (Dullien, 1992). However, the samples in carbonated rocks often present heterogeneities at core scale because of the presence of the secondary porous system i.e. fractures and vugs. It is clear that in the presence of fractures and/or vugs the conventional “homogeneous” interpretations of the experiments cannot be used directly, since the main hypothesis of the sample homogeneity is violated.

Many laboratory works have attempted to characterize the flow properties of vuggy structures. Ehrlich (1971) measured the permeabilities of vugular cores and he found that the global flow properties are very different from the properties corresponding to the microporosity; he proposed a mathematical model to interpret the experimental results to predict realistic reservoir flow properties. DeZabala et al (1995) studied waterflood in a vugular carbonate; they found that the porosity and permeability distributions are dissimilar; conventional interpretation methods were found inadequate. Dauba (1998) interpreted transient production data in order to get relative permeability curves from a vuggy core; the anomalous behavior could be associated to the small-scale heterogeneities. Kamath et al (1998) presented a study using a network model to improve the laboratory experiments interpretation in vugular samples. They found that pore network models helped improving analysis of experimental results where the conventional approach was inadequate. However the establishment of a calibration process would need further study. Moctezuma et al (1999) studied a vugular structure using tracer dispersion technique and history matching trying to characterize the permeability map from CT porosity maps at core scale. They found that the preferential path of flow observed in these types of cores can be matched with a matrix-vug permeability contrast but the value is depending on the scale. Kamath et al (2001) tried to understand the behavior in carbonates cores in terms of residual oil saturation by using flow visualization for different structure carbonate samples. They found that, depending on the structure, the pressure gradient used in waterfloods and the pore-throat aspect ratio might influence severely the residual oil saturation.

The objective of the present paper is to interpret water-oil relative permeabilities in vuggy porous media analyzing them in terms of pore structure characteristics. Two outcrop rocks with comparable porosity and formation factor but very different geometrical structure were studied. Water-oil displacements (forced imbibition and secondary drainage) were conducted, and relative permeabilities were determined through 1D history matching simulations. The paper is divided in two parts, an experimental and a numerical modeling part. In the first, the description of the samples,

the experimental conditions and the displacement results are studied. In the second, numerical 1D single and double porosity simulations are presented and the analysis in terms of relative permeabilities.

EXPERIMENTATION

Thin Sections

The samples have been selected on the basis of visual geometrical criteria on 2D pore space images. They have a high pore size macropores/micropores contrast as well as a fair porosity and permeability (Bousquie, 1979). Description of the selected samples is given in Fig. 1 along with the pore structure images obtained by Cryo-SEM technique. In the following "ESTA" denotes Estaillades limestone and "BRAU" Brauvilliers limestone.

Pore-size Distributions (Mercury Injection) and Capillary Pressure (Pc) Curves

Fig. 2a shows the results of mercury injection for the two samples in terms of differential pore volume as a function of the minimum access radius (throats/thresholds) to the pores. The macroporosity system has pores as large as 1mm; connectivity between pore systems seems to be very different, tortuosity for sample BRAU is three times higher than the tortuosity of sample ESTA. The cut-off value for the systems is between 1 and 3 μm. The bimodal character of the pore structure for both samples is very well depicted. Note that sample ESTA is considered as a homogeneous rock.

Capillary pressure curves were obtained for a water-oil system with the centrifuging technique, both for imbibiton and second drainage. Fig. 2b presents the Pc as a function of the wetting phase saturation.

CT Scan Mapping

Using CT scan technique, local porosity (ϕ) maps were evaluated at maximum CT-scan resolution (voxel size of 0.117x0.117x1 mm); the porosity map by slice is evaluated with a matrix of 512x512 pixels and 197 slices. Fig. 3 shows one slice of porosity map, the porosity distribution, and the porosity profile along the core for both samples.

Displacement Experiments

Forced imbibition and forced drainage water-oil displacements were carried out on each sample (20cm in length and 5cm in diameter). The fluids used were brine 25g/l KCl and low viscosity oil, Soltrol 130 (1.4 cp). The experimental saturation conditions are presented in Table 1. During displacement fluid production was recorded and local saturation distributions were measured using X-ray CT-scan technique. Saturation at each pixel was evaluated by the formula

$$\left(S_w\right)_{ij}\Big|_k = 1-\left(\left[CT_{100w}-CT\right]/\left[CT_{100o}-CT_{100w}\right]\right)_{ij}\Big|_k = 1-\left(S_o\right)_{ij}\Big|_k \qquad (1)$$

where the subscripts 100o and 100w correspond to the CT number for the porous medium fully saturated with oil and water respectively. In all the related figures, the average profiles are present in terms of injection phase saturation (water for imbibition, oil for drainage). The time for each profile increases from bottom (initial condition) to the top.

Since the injection rate for all the experiments was set to 50 cc/hr, the capillary number was of the order of 10^{-6} and viscosity instabilities were avoided. The inlet pressure,

temperature, oil and water productions were continuously registered in a computer. CT-scan acquisition was done at different times. Fluid injection was maintained until the displaced fluid production was stopped.

Forced Imbibition Displacement

Initial Conditions for S_{wi}

At the beginning each sample was 100% saturated with brine and its permeability was measured. Then, high viscosity oil (52 cp) was injected at low rate, 3 cc/hr. The oil flowrate was progressively increased until no more brine production was observed for the maximum permissible inlet pressure value. For a maximum pressure of 28 bars, final S_{wi} of 40% and 34% were achieved for samples BRAU and ESTA respectively. Then, the high viscosity oil was replaced by oil (1.4 cp) by injecting several pore volumes at low flow rate, 5 cc/hr. The viscosity at the outlet was controlled to confirm that the viscous oil was totally replaced. Rate was then increased at 500cc/hr and an effective permeability to oil $K_o(S_{wi})$ (110mD for sample BRAU and 214mD for sample ESTA) was measured.

Kinetics of Displacement

Fig. 4 presents the differential pressure and production data. It is interesting to note that breakthrough (BT) occurred very rapidly for sample BRAU (at 24min and 0.16 pore volume). After BT the oil production remained high (at BT only 46% of totally produced oil had been recovered). This behavior is unusual for imbibition displacements in homogeneous water-wet rocks. Contrary to BRAU, sample ESTA presented typical imbibition characteristics of rather homogeneous rocks with a fast initial oil production that stopped abruptly after BT (at BT 95% of totally produced oil had been recovered). Figure 4 also presents the simulation results of 1D history matching, which will be commented in the simulation section.

Saturation Profiles

The saturation profiles are presented in Fig. 5. It is interesting to note that the profiles for sample BRAU are radically different from the ones in sample ESTA. Saturation profiles in sample BRAU are very evocative of two parallel and interconnected pore structures; the macropores/vugs on one side and the micropores/matrix on the other. They are almost flat indicating that the early breakthrough can be associated to water flow through a main high permeability system (highly interconnected pathway consisting of macropores/vugs). After BT, this high permeability system is fed with oil coming from the micropore structure, in which oil remains continuous and water/oil displacement continues long after the water BT. In sample ESTA a piston like displacement has been detected, characteristic of a homogeneous core. It is believed that the macropores/vugs in ESTA sample are not well interconnected. Only accessible through the matrix, they constitute important oil reservoirs but also oil traps, since oil remains isolated there once the matrix is invaded by water.

Secondary Drainage Displacements

Initial Conditions at S_{or}

At the end of the forced imbibition experiments described above, injection of water has continued at different and increasing flowrates in order to produce all the recoverable oil.

When the residual oil saturation, S_{or}, was achieved, a CT-scan profile was done that serves as initial saturation profile for the secondary drainage experiment. During oil injection displacement, fluid production, pressures and saturation profiles were monitored in the same way as in the imbibition experiments.

Kinetics of Displacement
Fig. 6 shows the differential pressure and fluid production data during the secondary drainage. Both samples present the characteristics of drainage in a homogeneous core with an early oil breakthrough accompanied by a long tail of water production. This behavior also confirms the water-wetness of the cores.

Saturation Profiles
The oil saturation profiles are presented in Fig. 7. Note that the profiles for both samples are quite similar after the oil breakthrough; they are rather flat indicating that water remains continuous and is produced from the whole structure. However, before BT, again a piston like profile can be distinguished in the ESTA sample.

NUMERICAL SIMULATIONS

1D numerical simulations (using ATHOS® the IFP's reservoir simulator) were performed considering uniform porosity, permeability and initial saturation along the core. History matching was conducted to get the relative permeability curves. Also, for sample BRAU, a double porosity model was used to analyze the oil production behavior and the saturation profiles.

1D Simple Porosity Model

Table 2 presents the main parameters used in the simulations. The results are shown in Figures 4 to 7. The solid lines correspond to the simulation results. A very good agreement between experiment and simulation is obtained.

Relative Permeability Hysterisis
The relative permeabilities used to obtain this fitting are given in Figure 8 for both forced imbibition and secondary drainage.

Sample BRAU exhibits strong hysterisis for both wetting (water) and non-wetting (oil) phase. During imbibition, the macropores/vugs are rapidly invaded by water leading to high K_{rw}, while oil relative permeability, K_{ro}, is dominated by the capacity of the matrix to send oil to the high permeability channel. This leads to rapidly decreasing K_{ro} values. During secondary drainage, K_{rw} decreases dramatically since water is replaced by oil in the high permeability channel and practically only the matrix contributes to the water flow. Simultaneously, K_{ro} increases.

For sample ESTA the hysterisis is less strong than for sample BRAU. Of course, the wetting phase flows more easily in imbibition than in drainage, where the most permeable pathways are invaded by the non-wetting phase. However, K_{ro} exhibits an unexpected hysteresis with the values at imbibition being higher than the values at drainage. This can be explained by thinking that during drainage many macropores, which contain trapped oil and are accessible only through the matrix, are not invaded by

the injected oil. Thus oil remains trapped there, contributing to the saturation, but not to the mobility of the phase.

Effect of the Structure on Relative Permeabilities

Fig. 9 shows a comparison of the relative permeability curves in the two samples for forced imbibition and secondary drainage. For forced imbibition, K_{rw} is higher in BRAU sample than in ESTA sample, while for K_{ro} the opposite is true. For the secondary drainage, K_{ro} is higher in BRAU sample, while again K_{rw} exhibits the opposite behavior. This is consistent with the idea that in BRAU sample two structures coexist which are very well interconnected; however, in the ESTA sample the macropores/vugs are only accessible through the matrix. Thus, in the BRAU sample the injected phase has always a higher permeability since it flows through the interconnected vugs pathway, while the expelled phase circulates less easily since it is confined to flow in the low permeability matrix.

1D Double Porosity Model

A numerical simulation study considering a double porosity model was conducted for the sample BRAU. The idea was to separate the porosity system in two sub-systems: "vugs" and "matrix". The numerical option of double porosity-simple permeability was used. It assumes matrix-vugs exchanges, which means that matrix feeds with fluids the main flow path, the "vuggy" system. Pc and K_r curves for each sub-system are considered separately. Based in mercury injection curves we deduced the capillary pressure contrast ($Pc_v/Pc_m=r_m/r_v$), the permeability contrast ($K_v/K_m=r_v^2/r_m^2$) and the fraction of porosity associated to each sub-system ($\phi=\phi_v+\phi_m$). Table 3 shows the main parameters used in the simulations. In Fig. 2a we can see that the matrix Pc is approximately 10^2 times higher than the one of the vugs system.

The S_{wi} and S_{or} values were considered the same for the two systems. Another parameter influencing the simulation is the "block size" for the matrix. In the present analysis, it is considered that there is only one matrix block in each cell, so its size is equal to the grid cell. Both Pc curves for each sub-system were fixed for the simulation. Then, the two sets of K_r were identified by history matching of the experimental measurements. The results of this simulation are presented in Fig. 10. It is seen that the experimental data are also very satisfactorily matched if, instead of running simple porosity simulations with "pseudo-homogeneous" K_r, the real structure of the rock is considered with realistic K_r for each homogeneous sub-system. The "vug" and "matrix" K_r are presented in Fig. 11, along with the "pseudo-homogeneous" K_r. It is seen that each sub-system's K_r are smooth functions of saturation, contrary to the "pseudo-homogeneous" K_r that contained discontinuities reflecting the heterogeneities hidden behind them.

CONCLUDING REMARKS

Forced imbibition and secondary drainage experiments have been performed in two limestones with bimodal throat size distribution and similar macroscopic properties but very different pore structures. It has been demonstrated that well connected macropore structures influence dramatically the displacement patterns mainly for imbibition conditions. In these systems the injected fluid starts by invading the high permeability

path, then the matrix is progressively emptied. When the macropores are poorly interconnected and accessible only through the matrix, the rock behaves globally rather as a homogeneous one.

1D single porosity simulations demonstrated that flow in this type of heterogeneous media can be simulated using "pseudo-homogeneous K_r" functions. These "pseudo-homogeneous K_r" will of course depend on the scale the measurement has been performed. 1D double porosity simulations showed that there exists at least one solution assuming that the heterogeneous rock is a superposition of two homogeneous systems with smooth curves for the corresponding K_r. This analysis might simplify upscaling of the laboratory measured K_r. However, more work is needed concerning the separation in two porosity subsystems and the uniqueness of the solution.

ACKNOWLEDGEMENTS

The authors wish to acknowledge P. Poulain for his help with the experiments and B. Zinszner for his help in choosing the samples and for fruitful and interesting discussions.

REFERENCES

1. Archie, G. E., "Classification of Carbonate Reservoir Rocks and Petrophysical Considerations", *AAPG Bulletin*, (1952), **36**, 278-298.
2. Bousquié P., *Texture et Porosité de Roches Calcaires*, PhD Thesis, Université de Paris VI, Paris, (1979).
3. Dauba, C, Hamon, G., Quintard, M. and Lasseux, D., "Stochactic Description of Experimental 3D permeability Fields in Vuggy Reservoir Cores", SCA 9828, *Society of Core Analysts* International Symposium, (1998), The Hague.
4. DeZabala, E.F. and Kamath, J., "Laboratory Evaluation of Waterflood Behavior of Vugular Carbonates", SPE 30780, presented in *SPE ATCE*, (1995), Dallas, TX, October 22-25.
5. Dullien, F. A. L., *Porous Media. Fluids Transport and Pore Structure*, Edit. Academic Press, Inc. Second edition, (1992).
6. Ehrlich, R., "Relative Permeability Characteristics of Vugular Cores- Their measurement and Significance", SPE 3553, presented *in 46th Annual SPE meeting of the Society of Petroleum Engineers of AIME*, (1971), New Orleans, La.
7. Kamath, J., Xu, B., Lee, S.H. and Yortsos, Y.C., "Use of Pore Network Models to Interpret Laboratory Experiments on Vugular Rocks", *Journal of Petroleum Science and Engineering*, (1998), **20**, 109-115.
8. Kamath, J., Nakagawa, F., Meyer, R., Kabir, S and Hobbet, R., "Laboratory Evaluation of Waterflood Residual Oil Saturation in Four Carbonate Cores", Proceedings, *Society of Core Analysts* International Symposium, (2001).
9. Lucia, F.J., *Carbonate Reservoir Characterization*, Berlin Heidelberg, Springer-Verlag. (1999).
10. Moctezuma-Berthier, A. and Fleury, M., "Permeability Mapping on Vuggy Core Sample Using Tracer Experiments and StreamLine Simulations", *Society of Core Analysts* International Symposium, (1999).
11. Moore, C. *Carbonate Reservoirs*, Elsevier. (2001), 444.

Table 1- Saturation conditions for the samples during displacements.

	IMBIBITION			DRAINAGE		
Sample	S_{wi}	S_w(@BT)	S_{wr}	S_{oi}	S_o(@BT)	S_{or}
BRAU	0.400	0.566	0.825	0.175	0.267	0.431
ESTA	0.339	0.783	0.817	0.183	0.363	0.510

Table 2- 1D Simple porosity simulation parameters.

Sample (66 cells in flow direction)	**ESTA**	**BRAU**
Water Density	0.997 g/cc	0.997 g/cc
Oil Density	0.77 g/cc	0.77 g/cc
Water viscosity	0.91 cp	0.91 cp
Oil viscosity	1.4 cp	1.4 cp
(1)Porosity	30%	33%
(1)Permeability	214 mD	115 mD

(1) Experimental values

Table 3- 1D Double porosity simulation parameters.

Sample BRAU (66 cells in flow direction)	**VUGS**	**MATRIX**
Density	0.997 g/cc	0.997 g/cc
Oil Density	0.77 g/cc	0.77 g/cc
Water viscosity	0.91 cp	0.91 cp
Oil viscosity	1.4 cp	1.4 cp
(2)Porosity	16.8%	16%
(2)Permeability	115 mD	0.0115 mD

(2) Hypothetical case

Sample BRAU:

Oobiosparite grainstone with macroporosity arround 0.20 (>1 μm) and micropores arround of 0.12. The macropores are divided in two classes; 0.14 are associated to intergranular pores and 0.06 associated to the intraoolitic pores.

- Permeability to:
  Air: 142 mD;
  Water: 115 mD
- Porosity: 0.328
- Formation factor: 17.62
- Tortuosity: 33.4

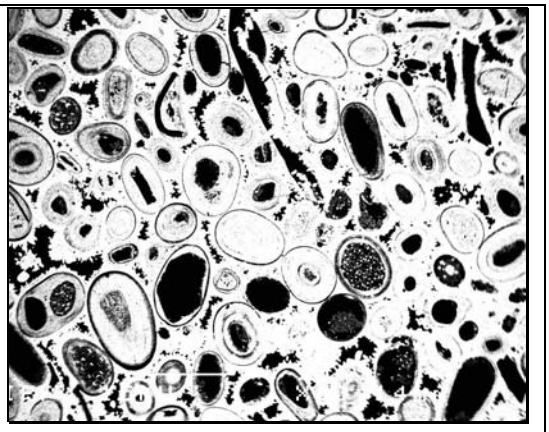

Sample ESTA:

Biosparite grainstone with intergranular porosity arround 0.18 (>1 μm) and micropores arround of 0.12. The macropores are characterized by a bimodal pore size distribution.

- Permeability to:
  Air: 246 mD;
  Water: 219 mD
- Porosity: 0.299
- Formation factor: 11.34
- Tortuosity: 11.49

1mm

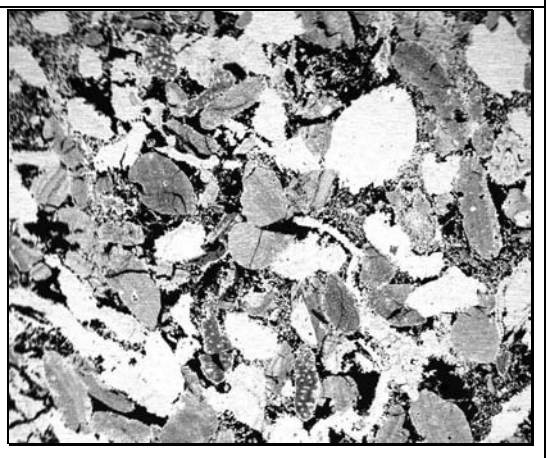

Figure 1. Sample description and CRYO SEM thin sections. Black corresponds to open pore space, gray can be associated to microporosity zones.

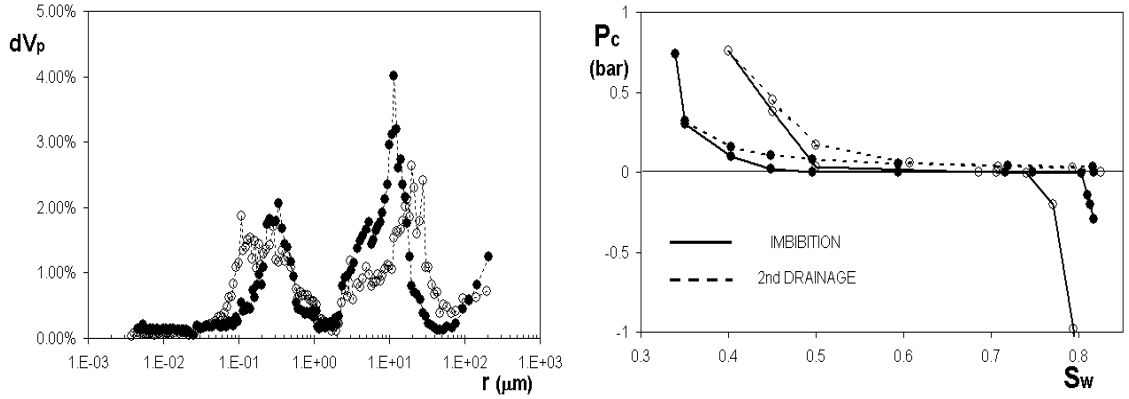

a) b)

Figure 2. (a) Mercury injection (Purcell method) results for pore volume as a function of the corresponding minimum access radius. (b) Oil-water centrifuge capillary pressure curves for imbibition and secondary drainage. Symbols (○) are for sample BRAU and (●) for sample ESTA.

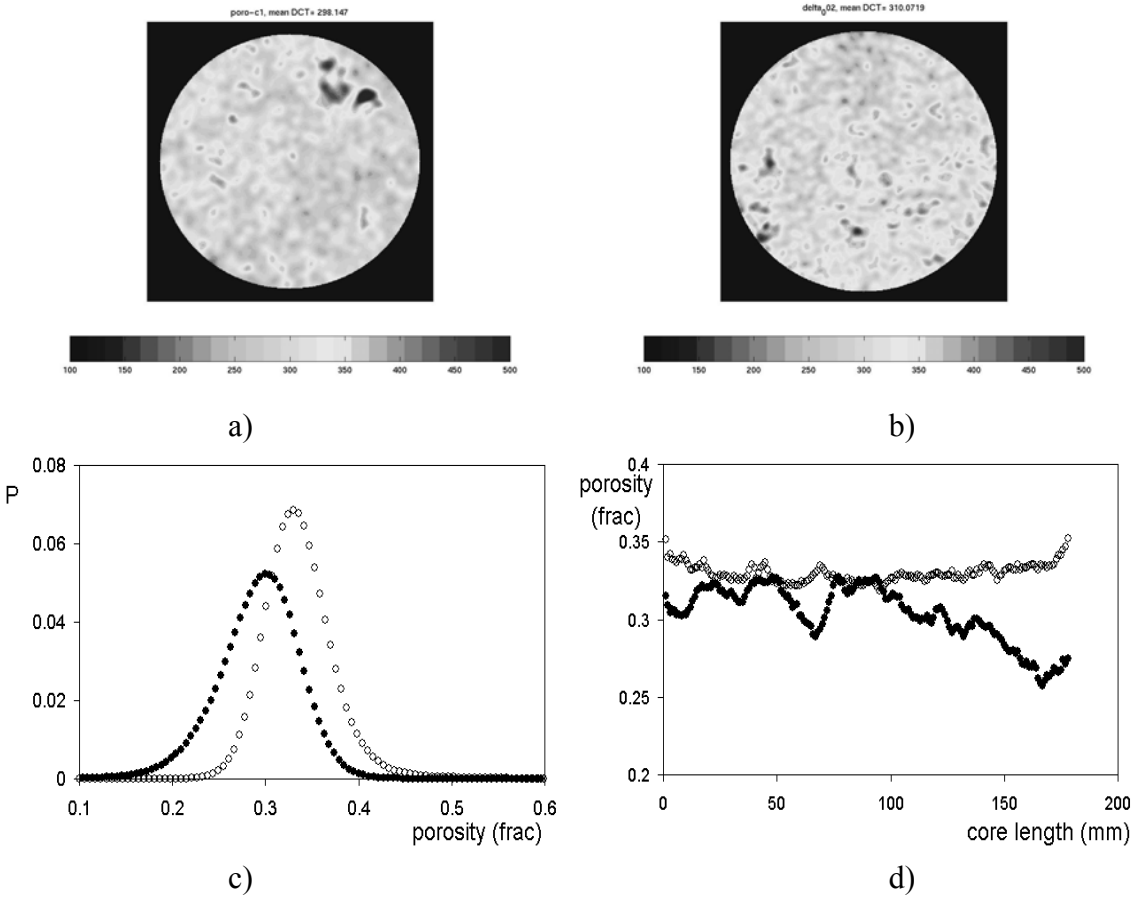

Figure 3. Example of porosity map image for a) sample BRAU and b) sample ESTA. Figure c) shows the probability histogram of porosity and figure d) the CT-scan porosity profile for the samples. Symbol (○) corresponds to sample BRAU and (●) to sample ESTA.

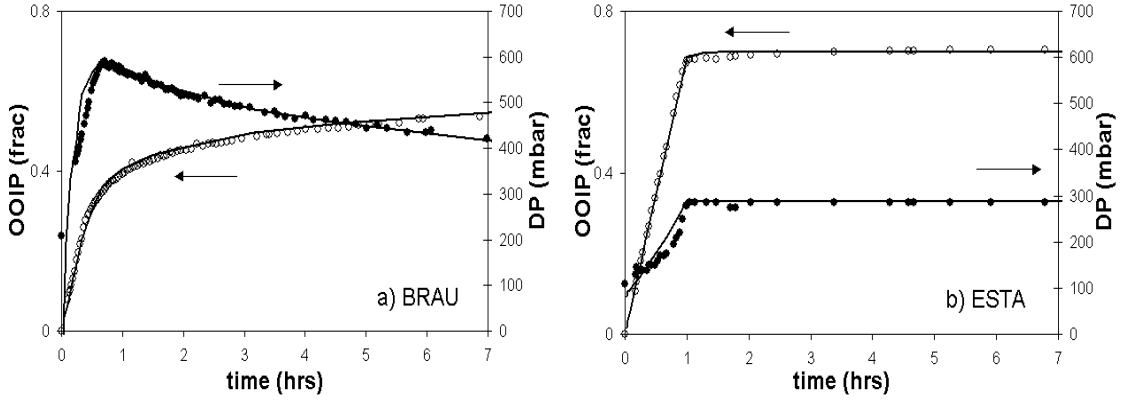

Figure 4. Kinetics of oil production (○) and differential pressure (●) for forced imbibition displacements. Solid lines correspond to the history matching obtained with 1D simple porosity simulations.

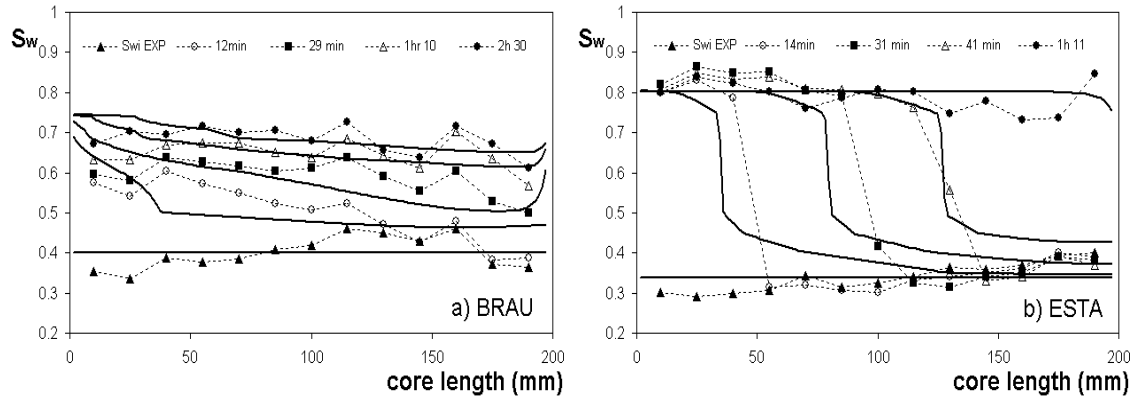

Figure 5. CT-scan water saturation profiles during forced imbibition displacements. Injection face is situated at the left side. Time in the profiles is increasing from bottom (initial condition) to the top. Solid lines correspond to the history matching obtained by 1D single porosity simulations

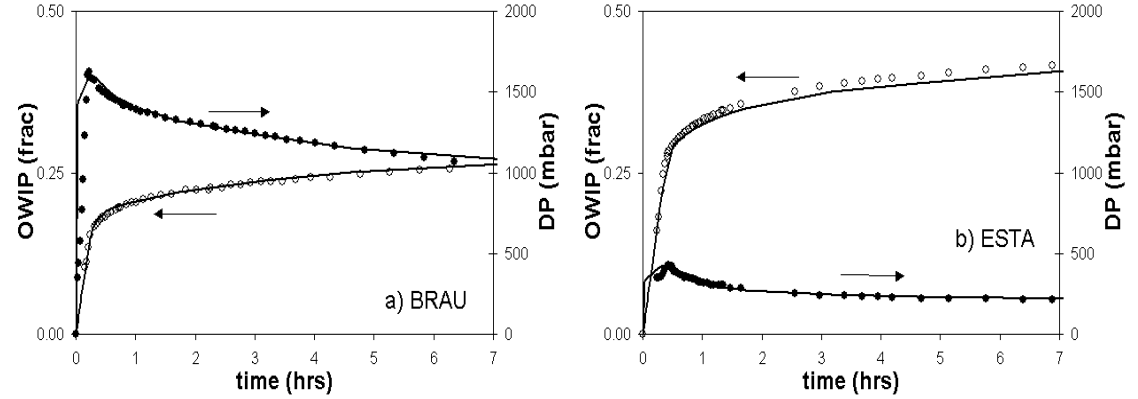

Figure 6. Kinetics of water production (○) and differential pressure (●) for forced drainage displacements. Solid lines correspond to the history matching obtained with 1D simple porosity simulations.

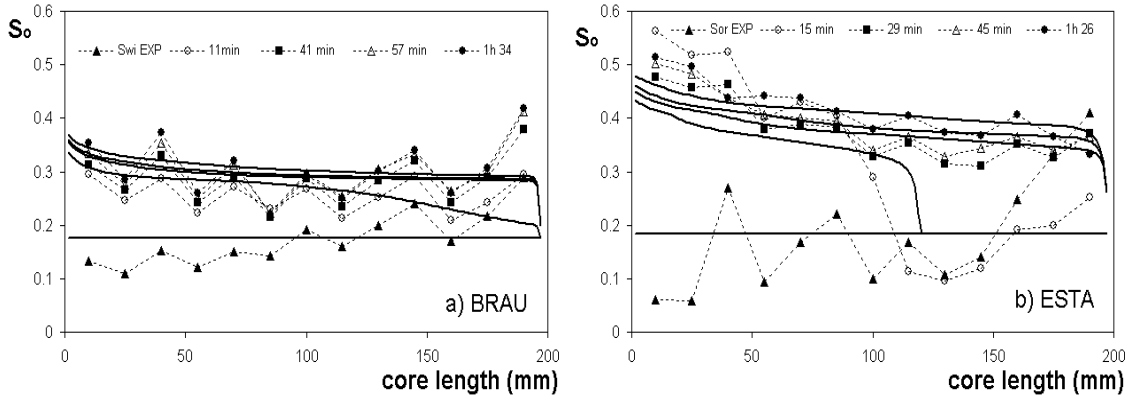

Figure 7. CT-scan oil saturation profiles during forced drainage displacements. Injection face is situated at the left side. In the profiles, time is increasing from bottom (initial condition) to the top. Solid lines correspond to the history matching obtained by 1D single porosity simulations.

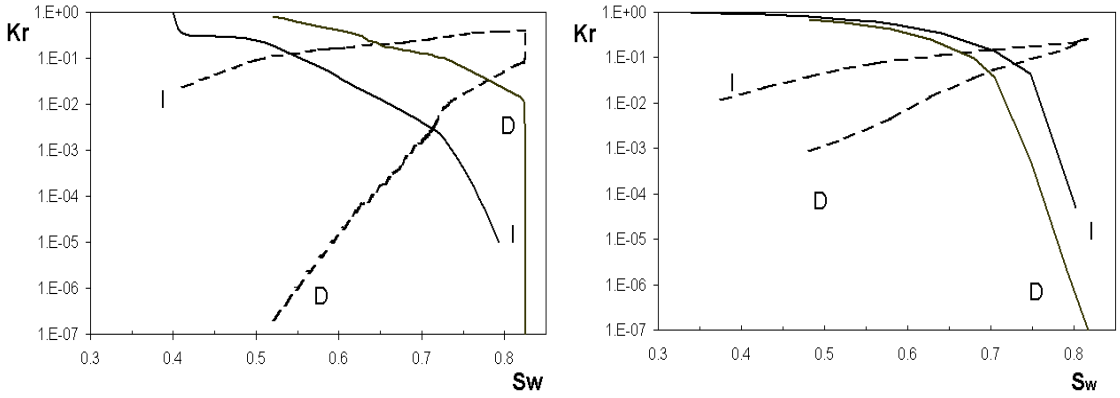

Figure 8. Relative permeability hysteresis for sample BRAU (left) and sample ESTA (right). Solid lines correspond to the oil phase. Dashed lines to the water phase. Letters I and D denote imbibition and drainage, respectively.

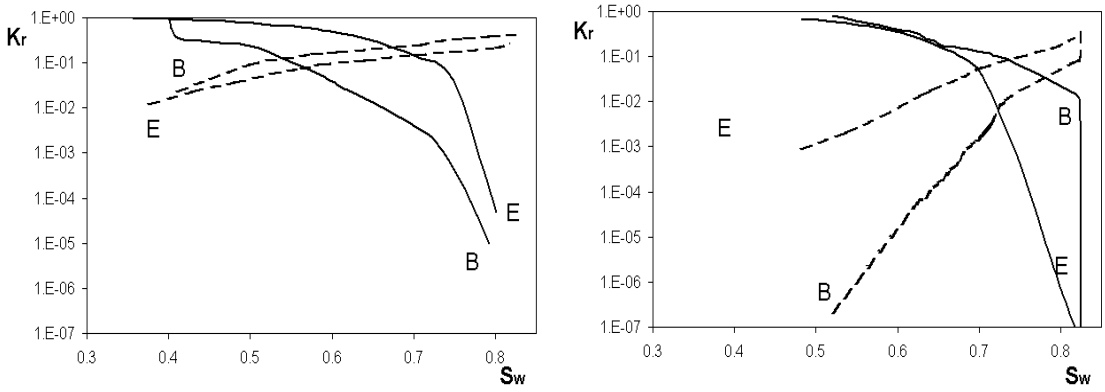

Figure 9. Comparison of the relative permeabilities in the two studied samples. For forced imbibition (left) and forced drainage (right) displacements. Solid lines correspond to oil phase. Dashed lines to water phase. Letters B and E correspond to sample BRAU and ESTA respectively.

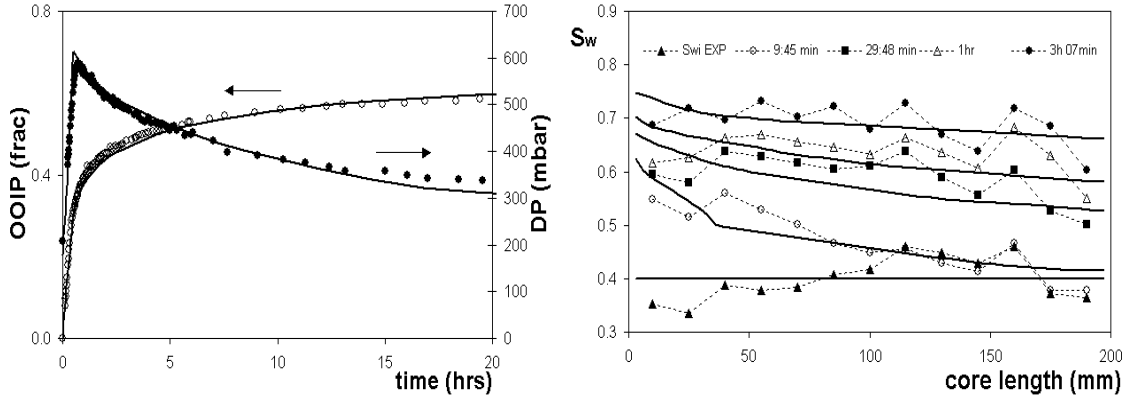

Figure 10. Kinetics (left) of oil production (○) and differential pressure (●). Saturation profiles (right) during forced imbibition displacement in sample BRAU. Time in the profiles increases from bottom (initial condition) to the top. Solid lines correspond to the history matching obtained by 1D double porosity simulations.

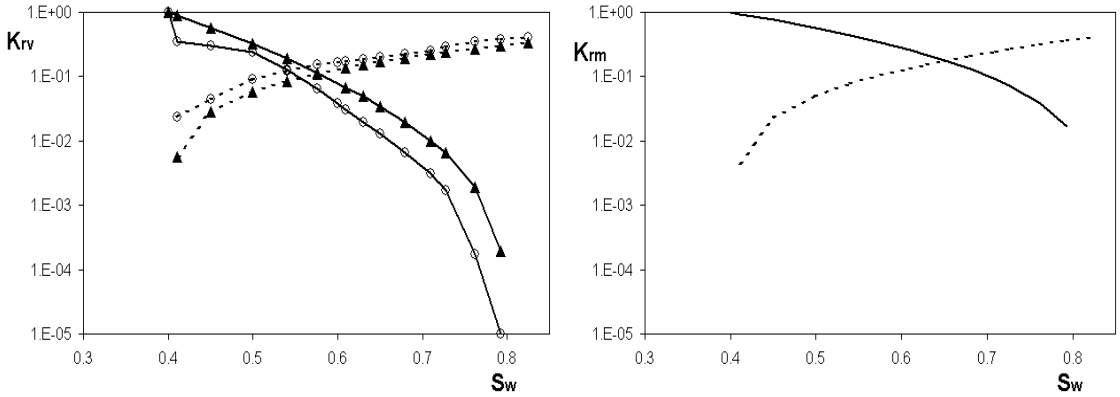

Figure 11. Relative permeabilities for forced imbibition in sample BRAU. Comparison between "pseudo-homogeneous K_r" obtained by simple porosity simulation (○) and Kr for the vuggy system obtained by 1D double porosity simulation (▲) (left). K_r curves (right) for the matrix system used in 1D double porosity simulation. Solid lines correspond to oil phase and dashed lines to water phase.